Indian Journal of Chemistry
Vol. 59A, June 2020, pp. 768-774

Photocatalytic activity of mixed-phase of TiO_2 synthesized by non-aqueous methodology

Pratibha V Bakre & Santosh G Tilve*
School of Chemical Sciences, Goa University, Goa 403206, India
Email: stilve@unigoa.ac.in

Received 24 February 2020; revised and accepted 22 April 2020

A mix-phase (anatase-rutile) nanocrystalline titania particles were successfully synthesized in a non-aqueous solvent medium using a novel approach of controlled hydrolysis of titanium isopropoxide. The hydrolysis was carried out by the controlled release of water molecules from simple Schiff base formation reaction of anisaldehyde employing aniline as an amine component in isopropanol solvent medium. The excess aniline used, and the imine formed acts as directing agents. The photocatalytic activities of the catalysts prepared were compared with Degussa P25 for methylene blue degradation in direct sunlight. The photocatalytic activity was found to increase with decreasing availability of water molecules formed during the Schiff base formation (imination) reaction. Also, it was found to affect the phase and shape selection. TEM images show sphere-like to hexagonal to a rod-shaped formation of particulates.

Keywords: Titanium dioxide, Sol-gel, Non-aqueous methodology, Photocatalyst

Nanostructured titanium dioxide (TiO_2) has gained much attraction and is intensively studied due to its potential applications in various fields such as photocatalysis, photovoltaic cells, textiles, paints, glass, ceramic, paper industries, cosmetics, medicine, *etc*[1-5]. The properties of TiO_2 mainly depend on the crystal structure, crystallite phase, surface characteristics, and the synthetic route used.

Various dyes; commonly known pollutants, are released from various industries such as textile, paper, fabric, leather and dyestuff production and extensive research is being done to find out better catalytic adsorbent material to degrade these dyes and hence reduce the risk of environmental pollution. TiO_2 is commonly studied adsorbent material for photo-degradation of such dyes.

Literature study reveals that for photocatalytic applications in environmental remediation, anatase TiO_2 is one of the most studied and a better polymorph out of the three commonly known crystalline phases of TiO_2[6-9]. However, it has a drawback in absorbing an insignificant amount of visible light due to its high band-gap. Improvement in the efficiency of the anatase TiO_2 can be achieved by defect engineering[10-11], surface doping[12-14], surface controlling, *etc.*[15-16]. Rutile phase of TiO_2 has a narrower band-gap compared to anatase TiO_2. However, it is found to be a poorer photocatalyst. One of the reasons for this lower activity could be higher temperature (>600 °C) required for the synthesis which results in more compactness of the crystals formed and also more aggregation resulting in a larger size and thereby lesser surface area[17-18]. In 1991 it was revealed that anatase-rutile mixed-phase shows enhanced photocatalytic activity[19]. This observation has led to efforts in phase controlling at a lower temperature[20-24]. A recent study has shown that non-aqueous solvothermal route yield anatase-rutile mixed-phase at relatively lower temperature and displays enhanced photocatalytic activity for the degradation of Rhodamine B under visible light[25].

Recently we studied mono-carboxylic, dicarboxylic and amino acids as templates in sol-gel synthesis of TiO_2 for improved properties, and also the role and effect of these acids on the properties[26-29]. It was observed that longer chain and sterically bulky acids produce phase pure anatase catalyst with higher surface area and smaller size displaying better photo-activity. In the case of dicarboxylic acids, the phase formation was found to be depending on the presence of functional groups in the acid precursor. In all these organic acids used, we observed that the formation of metal carboxylate bonds is perhaps the controlling factor during the hydrolysis and condensation process leading to gel formation. Further, the non-hydrolytic decomposition during calcination controls the phase

formation. While in the case of amino acids used in excess, we found that the acid acts as surfactant and may not be participating by the formation of a metal carboxylate bond. In continuation of our search for better photocatalyst, we report herein the synthesis of anatase-rutile mixed-phase catalyst by a non-aqueous route using a novel approach of controlled hydrolysis of titanium isopropoxide. Here we have exploited the organic imination reaction (Schiff base formation) route for the controlled release of water. In literature, organic esterification as a non-aqueous route has been exploited for releasing a controlled amount of water [25, 30-34].

It was expected that aniline would react with anisaldehyde to generate water, which would then hydrolyze the titanium isopropoxide (TIP). The hydrolysis reaction was to be controlled by the presence of water available, which could result in partial hydrolysis and polymerization sequences to form the gel, as shown in Scheme 1. The ratio of the aniline: anisaldehyde was varied to make available 4, 3 and 2 moles of water per mole of TIP. During the formation of a gel, imine and primary amine (aniline) could also serve as a directing ligand. The gel was then solidified and calcined at 500 °C for 3 h. During calcination, the surface isopropoxide groups are lost in a non-hydrolytic pathway. There are a few recent reports of imine (Schiff base) and amines as ligands in the hydrothermal synthesis of TiO_2. They were found to be effective to control the shape, size and optical properties[35-44].

Materials and Methods

In a typical synthesis, aniline (8 mL, 87.62 mmol) was mixed in isopropanol (50 mL) and to this mixture titanium (IV) isopropoxide (5 mL, 16.48 mmol) diluted with isopropanol (30 mL) was added with constant stirring. Anisaldehyde (8 mL, 65.81 mmol) in isopropanol (20 mL) was then added dropwise with constant stirring. The entire mixture was allowed to stir for further 2 h, which resulted in a white homogeneous colloidal solution. The reaction mixture was stirred further 12 h to form a gel. The gel was centrifuged at 5000 rpm. The residue was washed with isopropanol (3 times) to remove the excess aniline and the imine. The resulted semisolid material was dried at 100 °C to get precursor powder, and was further calcined at 500 °C for 3 h to produce the desired TiO_2 nanopowder. The resultant catalysts were labelled according to the varied ratio of precursors. The molar ratio of TIP: aniline: anisaldehyde was 1:5:4, 1:4:3 and 1:3:2. The same volume of TIP was maintained throughout the reaction. The samples are labelled according to the varied ratio of precursors are given in Table 1.

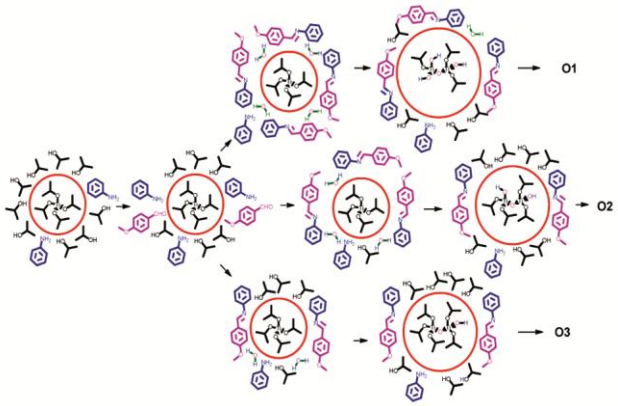

Scheme 1 — Probable course of gelation

The Infrared spectra of these samples were recorded using Shimadzu IR Prestige-21 FTIR in the range of 4000–400 cm^{-1}. Powder X-ray diffraction patterns were obtained with Mini Flex II, Rigaku, Japan diffractometer using Cu Kα radiation (λ= 1.5418 Å) radiation at a scanning speed of 2 °/min. Nitrogen adsorption/desorption isotherms were obtained using Quantachrome ASiQwin Instruments (ASIQC0100-4) at 77 K. Prior to gas adsorption the samples were degassed for 0.5 h at 300 °C. Morphology of the sample was investigated by using Zeiss Avo18 scanning electron microscope (SEM) instrument and TECHNAI F30 field emission transmission electron microscope (TEM), operating at 200 kV. UV-visible diffuse reflectance (DRS) spectra were recorded on Shimadzu UV-2450 Spectrophotometer. $BaSO_4$ was used as a background standard.

The photocatalytic activity of each sample was measured in terms of the degradation of methylene blue under sunlight irradiation. The experiment was carried out in bright sunlight for 120 min between 10:00 am to 12:00 noon. In a typical experiment, 10 mg of TiO_2 catalyst was suspended in 25 mL of the aqueous Methylene Blue dye solution (0.010 g/L) and

Table 1 — Sample labelling

TIP: Aniline : Anisaldehyde	Label
1 : 5 : 4	O1
1 : 4 : 3	O2
1 : 3 : 2	O3

kept in the dark overnight to allow adsorption of dye on catalyst if any. The solution was then exposed to sunlight for the duration of the experiment under intermittent swirling. After every 20 min interval, 2 mL aliquots were pipetted out centrifuged and the absorbance of the clear supernatants was determined at the wavelength 660 nm against appropriate blanks. The intensity of degraded dye was measured by using a colorimeter.

Results and Discussion

Phase and phase composition

X-Ray Diffraction studies were used to investigate the phase structure of the prepared TiO_2 samples. Fig. 1 shows the XRD patterns of the samples O1, O2 and O3 with the expanded region in the inset. The appearance of sharp peaks indicates the highly crystalline nature of all three samples. The major patterns for all the samples can be indexed to the anatase phase of TiO_2 with (101) peak of highest intensity. No brookite phase was seen in any of the samples. The weight fractions of anatase and rutile phase present in the samples were estimated based on the highest intensity peak of each phase (anatase and rutile) according to the Eqn 1.

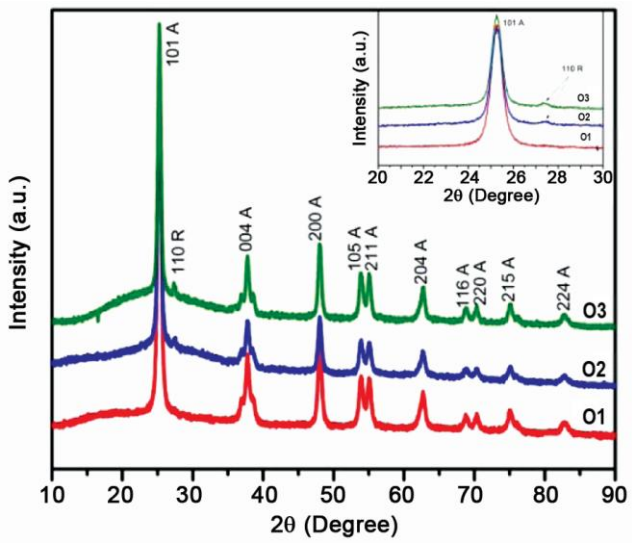

Fig. 1 — XRD plots for calcined samples.

$$\%A = \frac{100}{1+1.33\left|\frac{I(R)}{I(A)}\right|} \quad ...(1)$$

The sample O1 displays pure anatase phase with no peaks of other phases of TiO_2. The sample O2 displayed mixed anatase: rutile phase with about 3.9 % of rutile phase indexed to (110) peak, while the sample O3 has 5.5 % rutile phase (expanded region in inset of Fig. 1). The above results indicate that with the diminishing amount of water made available for the hydrolysis of TIP, the percentage of rutile phase increase. By further analyzing the XRD patterns, the average crystallite size was calculated from the line broadening of the highest intensity anatase (101) diffraction peak for all the samples, by using the Scherrer's Eqn 2.

$$D = K\lambda/\beta\cos\theta \quad ...(2)$$

Where, K is the Scherrer constant, λ is the X-ray wavelength, β is the peak width at half maximum and θ is the Bragg's diffraction angle. The crystallite size was found to be in the range of 13-15 nm (Table 2). The crystallite size of the particulate was found to increase with lesser the amount of water available as the relative percentage of rutile phase was increasing. This is in conformity with literature wherein the relative size of the rutile phase is always found to be greater than the anatase phase.

IR and diffuse reflectance spectroscopy

The prepared catalysts were studied by FTIR analysis. The IR spectra of samples O1, O2, O3 are shown in Fig. 2. Broad band at 3500-3000 cm^{-1} (-OH stretching) and ~1630 cm^{-1} (-OH bending) were seen for the surface hydroxyl and the adsorbed water. Strong band seen at 800-450 cm^{-1} was assigned for Ti-O stretching. No bands due to the organic part were discernible suggesting complete removal of the isopropoxy part attached to the titanium. Optical studies were carried out with the help of UV-visible DRS. Fig. 3 shows the UV-DRS spectra of samples. Here a steep decrease in the absorption at wavelengths longer than 380 nm is observed, which can be assigned to the intrinsic band-gap absorption

Table 2 — Summary of the properties of TiO_2 nanoparticles

Sample	Particle Size (nm)	Crystallite Size (nm)	BJH surface area (m^2/g)	Pore volume (cc/g)	λ_{max} (nm)	Rate constant k (min^{-1})
O1	8.5	12.9	50.0	0.073	392	0.0244
O2	10.0	13.4	44.5	0.068	396	0.0294
O3	10.4	15.3	33.3	0.051	398	0.0308
P25	21.0	25.0	56.0	0.250	370	0.0214

of pure anatase TiO_2. A slight red shift in absorption edge is observed as we move from sample O1 to O3, which could be due to an increase in rutile percentage in the samples. This is further confirmed from the decreasing band gap values of the samples which are found to 3.16, 3.13 and 3.11 eV, respectively.

BET surface area analysis

Fig. 4 illustrates the nitrogen adsorption-desorption isotherms and corresponding pore size distribution curves (inset) of the synthesized TiO_2 photocatalysts. The isotherms of these photocatalysts exhibited type-IV pattern typical of mesoporous materials. Slightly broader hysteresis with loop intermediate between H2- and H3-type is observed. The loops, closing at lower relative pressure and extending up to unity are indicative of the presence of mesoporosity and non-rigid structure of pores. Mesoporous nature is also seen from the broad pore size distribution of

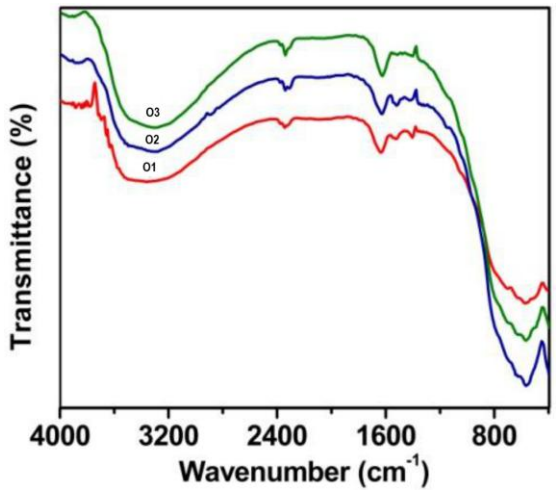

Fig. 2 — FTIR spectra of calcined samples.

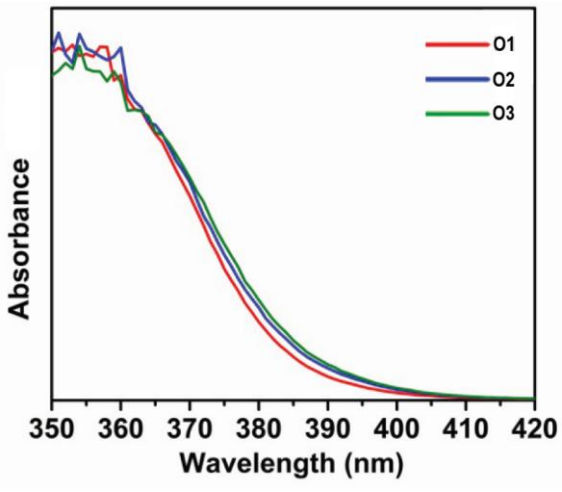

Fig. 3 — UV-DRS spectra of calcined samples.

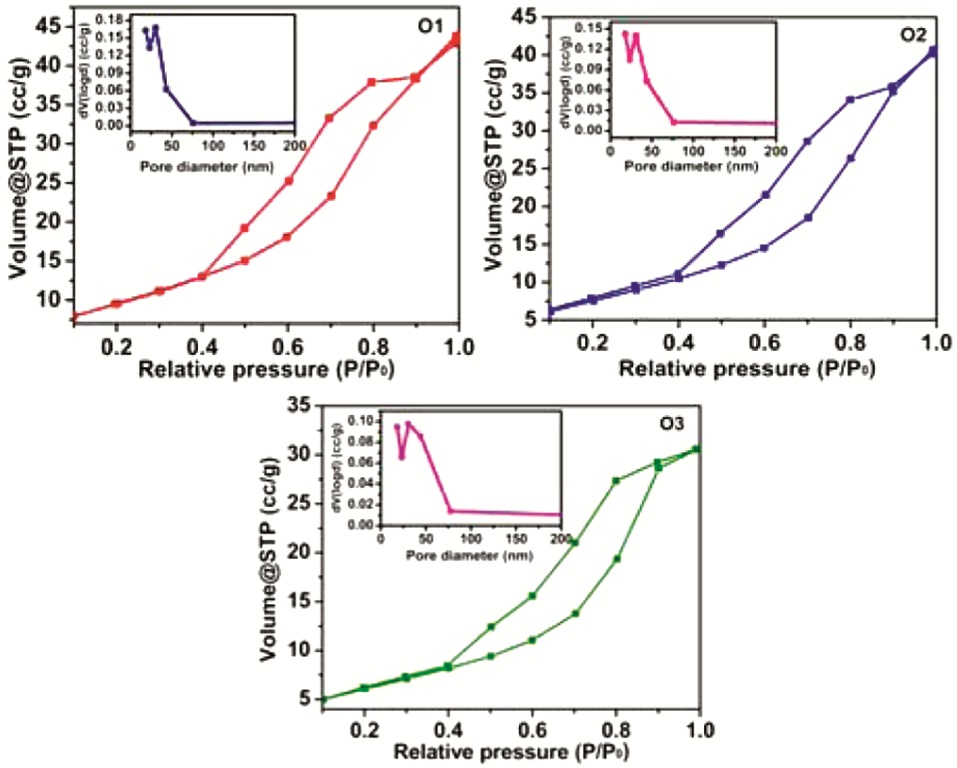

Fig. 4 — Nitrogen adsorption-desorption isotherms of TiO_2 nanoparticles.

these samples ranging from 20-80 nm (Table 2). Besides, the observed shift in hysteresis loops to the higher relative pressure region is also indicative of the capillary condensation associated with large pore channels[45]. The lower value of the specific surface area and pore volume for sample O2 and O3 can be attributed to the presence of a slight rutile phase in the samples which was also reflected in their crystallite and particle size.

Morphological analysis

Morphological studies were carried out using SEM analysis. The SEM micrographs, (Fig. S1, Supplementary Data) shows a well-defined densely packed tiny nanoparticle of spherical shapes for all the three samples. Slight agglomeration is observed for samples O2 and O3 while a comparatively higher degree of agglomeration is seen for the sample O1, which differentiate it from the other two samples. This difference is reflected in the photocatalytic activity and other characteristic properties of these samples.

Representative TEM images are shown in Fig. 5. The spherical shape of particles is confirmed from the TEM micrographs. In addition to the spherical particles, a few hexagonal and rod-shaped particles are seen in O2 and O3 samples, respectively (Fig. 5 insets, left corner bottom) which contain slight rutile phase. The spherical particles could be due to the anatase phase, and the hexagonal and rod-shaped could be of rutile phase as observed by Liu *et al.*[46] The average particle size was estimated to be about 8-10 nm with increasing size from O1 to O3 consistent with the XRD data (Table 2). The SAED pattern is shown in the inset of Fig. 5 (top right corner). A set of diffraction rings is observed in the SAED pattern indicating the polycrystalline nature of the catalysts prepared. The ring patterns could be indexed to anatase phase of TiO_2. Sample O3 displays discrete crystalline phases of TiO_2 because of higher percentage of rutile phase while other two samples display somewhat lesser crystallinity. The hexagonal and rod shape of some of the particles could be the result of the presence of the Schiff base and the amine in the medium (Scheme 1).

Photocatalytic activity

To evaluate the photocatalytic activity of the prepared TiO_2 nanoparticles, the activity of these samples was compared with that of the commercial

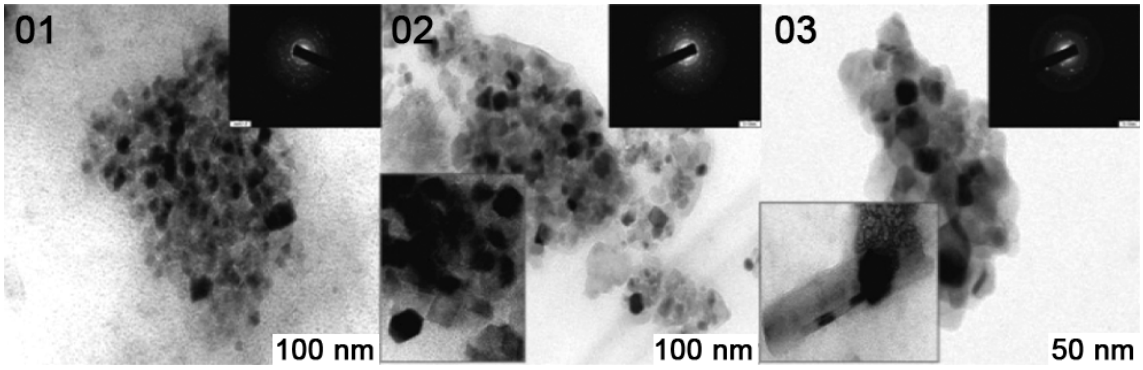

Fig. 5 — TEM images and corresponding SAED patterns (inset) of TiO_2 nanoparticles.

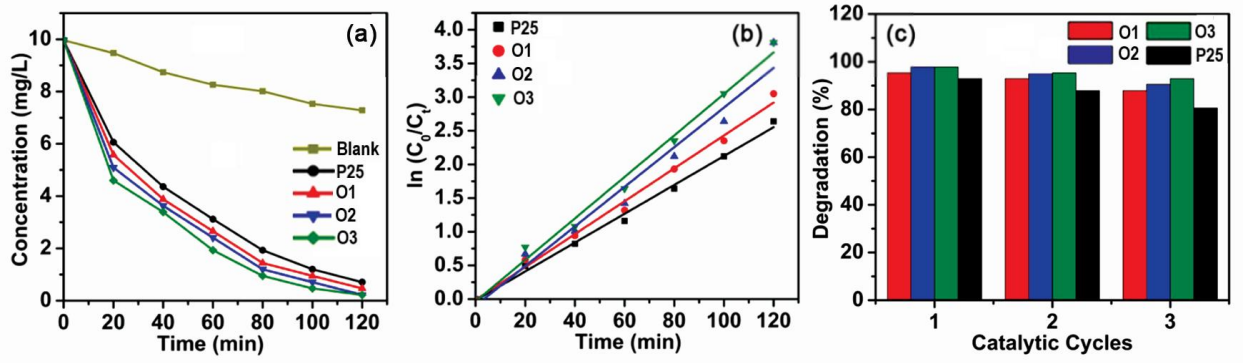

Fig. 6 — (a) degradation plots and (b) kinetic studies and (c) recyclability studies of the catalysts (O1, O2, O3 and P25) for the degradation of methylene blue in presence of sunlight.

Degussa P25 TiO_2 catalyst in the photo-degradation of methylene blue under direct sunlight. Natural sunlight has more practical relevance as it relates to on field process. Blank experiments were carried out to show that the photo-degradation reaction did not proceed effectively without the presence of a catalyst. The experiments were carried out thrice, and the average results are depicted in Fig. 6a.

It is found that all three samples show better photocatalytic activity in comparison to commercial Degussa P25 (Fig. 6a). Further, the results indicate that the samples having anatase-rutile mixture (O2 and O3) shows better photo-activity than the sample with pure anatase phase (O1). Amongst the catalyst prepared, sample O3 shows the best activity. The obtained results are consistent with the higher shift in absorption wavelength and the smaller size of these samples. Moreover, the improved photocatalytic activity of the samples O2 and O3 suggest that there is better utilization of the direct sunlight by catalyst having a slight rutile phase.

Further, the kinetics of dye degradation was studied to determine the rate of degradation. A plot of ln (C_0/C_t) versus time (Fig. 6b) represents a straight line which indicates the photocatalytic degradation follows a pseudo first order kinetics. Linear relationships for all the photocatalysts is seen from which it can be observed that the apparent reaction rate constant is highest for sample O3. The rate constant k for all three samples is defined by the Eqn 3

$$kt = ln\left(\frac{C_0}{C_t}\right) \quad ...(3)$$

and are given in Table 2, which is consistent with the other results. Recyclability studies for these samples were carried out for three cycles, after separating the catalysts by centrifugation. The results were compared with Degussa and are displayed in Fig. 6c. All the prepared samples could be reused for degradation with negligible loss in their activity. In our earlier studies, we had observed by COD studies that there is complete degradation of MB and by LC-MS that during photodegradation first oxidation of sulfur to sulfone takes place followed by *N*-demethylation, hydroxylation, and ultimately to complete demineralization[26,29].

Conclusions

In summary, a simple new method to develop TiO_2 nanoparticles *via* a non-aqueous sol-gel route by controlled release of water *via* imination reaction is reported. Anatase or mixed anatase-rutile phase can be controlled by varying the amount of release of water during the imination process. The excess used amine, aniline, and the *in-situ* formed corresponding Schiff base acts as directing agents to control the size and shape of the particulates. The photo-degradation results indicate that all the catalyst prepared by the present non-aqueous route shows better activity compared to the commercial Degussa P25. Among the catalyst synthesized the one obtained *via* the least amount of water released during the imination reaction had the best photocatalytic activity and had mixed anatase-rutile phase. Furthermore, the distinct red shift in the absorption edge compared to Degussa P25 contributed to the enhancement in the activity of the catalysts.

Supplementary Data

Supplementary data associated with this article are available in the electronic form at http://www.niscair.res.in/jinfo/ijca/IJCA_59A(06)768-774_SpplData.pdf.

Acknowledgment

Pratibha V Bakre thanks the UGC, New Delhi for the award of BSR Junior Research Fellowship and Senior Research Fellowship.

References

1 Borgarello E, Kiwi J, Pelizzetti E, Visca M & Gratzel M, *Nature*, 289 (1981) 158.
2 Zou Z, Ye J, Sayama K & Arakawa H, *Nature*, 414 (2001) 625.
3 Hoffmann M R, Martin S T, Choi W & Bahnemann D W, *Chem Rev*, 95 (1995) 69.
4 Cargnello M, Gordon T R & Murray C B, *Chem Rev*, 114 (2014) 9319.
5 Liu L & Chen X, *Chem Rev*, 114 (2014) 9890.
6 Tanaka K, Capule M F V & Hisanaga T, *Chem Phys Lett*, 187 (1991) 73.
7 Ohno T, Sarukawa K & Matsumura M, *J Phys Chem B*, 105 **(**2001) 2417.
8 Ohno T, Sarukawa K & Matsumura M, *New J Chem*, 26 (2002) 1167.
9 Prieto-Mahaney O -O, Murakami N, Abe R & Ohtani B, *Chem Lett*, 38 (2009) 238.
10 Gordon T R, Cargnello M, Paik T, Mangoline F, Weber R T, Fornasiero P & Murry C B, *J Am Chem Soc*, 134 (2012) 6751.
11 Liu G, Yu J C, Lu G (M) Q & Cheng H –M, *Chem Commun*, 47 (2011) 6763.

12 Mahy J G, Lambert S D, Léonard G L-M, Zubiaur A, Olu P -Y, Mahmoud A, Boschini F & Heinrichs B, *J Photochem Photobiol A*, 329 (2016) 189.
13 Devi L G & Kavitha R, *RSC Adv*, 4 (2014) 28265.
14 Lu X, Mou X, Wu J, Zhang D, Zhang L, Huang F, Xu F & Huang S, *Adv Funct Mater*, 20 (2010) 509.
15 Choi J, Sudhagar P, Lakshmipathiraj P, Lee J W, Devadoss A, Lee S, Song T, Hong S, Eito S, Terashima C, Han T H, Kang J K, Fujishima A, Kang Y S & Paik U, *RSC Adv*, 4 (2014) 11750.
16 Fei J & Li J, *Adv Mater*, 27 **(**2015) 314.
17 Hanaor D A H & Sorrell C C, *J Mater Sci*, 46 (2010) 855.
18 Zhang J, Zhou P, Liub J & Yu J, *Phys Chem Chem Phys*, 16 (2014) 20382.
19 Bickley R I, Carreno T G, Lees J S, Palmisano L & Tilley R J D, *J Solid State Chem*, 92 (1991) 178.
20 Xu F, Xiao W, Cheng B & Yu J, *Int J Hydrogen Energy*, 39 (2014) 15394.
21 Luo Z, Poyraz A S, Kuo C H, Miao R, Meng Y, Chen S Y, Jiang T, Wenos C & Suib S L, *Chem Mater*, 27 (2015) 6.
22 Shi L & Weng D, *J Environ Sci*, 20 (2008) 1263.
23 Honaor D A H, Chironi I, Karatchevtseva I, Triani G & Sorrel C C, *Adv Appl Ceram*, 111 (2012) 149.
24 Bagheri S & Julkapli N M, *Rev Inorg Chem* 31 (2016) 1.
25 Xu H & Zhang L, *J Phys Chem C* 113 (2009) 1785.
26 Bakre P V, Volvoikar P S, Vernekar A A & Tilve S G, *J Colloid Interface Sci*, 474 (2016) 58.
27 Bakre P V & Tilve S G, *ChemistrySelect*, 2 (2017) 7063.
28 Bakre P V, Tilve S G & Ghosh N N, *Monatsh Chem*, 149 (2018) 11.
29 Bakre P V & Tilve S G, *J Phys Chem Solids*, 116 (2018) 234.
30 Li H, Shen X, Liu Y, Wang L, Lei J & Zhang J, *J Alloys Compd*, 646 (2015) 380.
31 Li G & Gray K A, *Chem Mater*, 19 (2007) 1143.
32 Xu H, Li G, Zhu G, Zhu K & Jin S, *Catal Commun*, 62 (2015) 52.
33 Joo J, Kwon S G, Yu T, Cho M, Lee J, Yoon J & Hyeon T, *J Phys Chem B*, 109 (2005) 15297.
34 Zhong Z, Ang T-P, Luo J, Gan H -C & Gedanken A, *Chem Mater*, 17 (2005) 6814.
35 Noori E, Mir N, Salavati-Niasari M, Gholami T & Masjedi-Arani, *J Sol-Gel Sci Technol*, 69 (2014) 544.
36 Mir N & Salavati-Niasari M, *Electrochim Acta*, 102 (2013) 274.
37 Mir N & Salavati-Niasari M, *Sol Energy*, 86 (2012) 3397.
38 Mir N & Salavati-Niasari M, *Mater Res Bull*, 48 (2013) 1660.
39 Masjedi M, Mir N, Noori E, Gholami T & Salavati-Niasari M, *Superlattices Microstruct*, 62 (2013) 30.
40 Gholami T, Mir N, Masjedi-Arani M, Noori E & Salavati-Niasari M, *Mater Sci Semicond Process*, 22 (2014) 101.
41 Kianfar A H, Dehghani P & Momeni M M, *J Mater Sci- Mater Electron*, 27 (2016) 3368.
42 Heydari-Bafrooei E, Amini M & Hatefi M, *Biosens Bioelectron*, 85 (2016) 828.
43 Sharma N, Sharma V, Bohra R & Raju V S, *Appl Organomet Chem*, 21 (2007) 763.
44 Gholami T, Bazarganipour M, Niasari M S, Hamadanian M & Bagheri S, *J Mol Liq*, 215 (2016) 467.
45 Leofanti G, Padovan M, Tozzola G & Venturelli B, *Catal Today*, 41 (1998) 207.
46 Liu X, Li Y, Deng D, Chen N, Xing X & Wang Y, *CrystEngComm*, 18 (2016) 1964.